**Sachin P. Budhabhatti**
Ph.D.
Department of Biomedical Engineering,
Cleveland Clinic,
Cleveland, Ohio 44195;
Department of Chemical and Biomedical
Engineering,
Cleveland State University,
Cleveland, Ohio

**Ahmet Erdemir**
Ph.D.
Department of Biomedical Engineering,
Cleveland Clinic,
Cleveland, Ohio 44195

**Marc Petre**
Ph.D.
Department of Biomedical Engineering,
Cleveland Clinic,
Cleveland, Ohio 44195;
Department of Biomedical Engineering,
Case Western Reserve University,
Cleveland, Ohio

**James Sferra**
MD

**Brian Donley**
MD

Department of Orthopaedic Surgery,
Cleveland Clinic,
Cleveland, Ohio 44195;
The Orthopaedics Research Center,
Cleveland Clinic,
Cleveland, Ohio 44195

**Peter R. Cavanagh**[1]
Ph.D. D.Sc.
Department of Biomedical Engineering,
Cleveland Clinic,
Cleveland, Ohio 44195;
Department of Orthopaedic Surgery,
Cleveland Clinic,
Cleveland, Ohio 44195;
The Orthopaedics Research Center,
Cleveland Clinic,
Cleveland, Ohio 44195
e-mail: cavanap@ccf.org

# Finite Element Modeling of the First Ray of the Foot: A Tool for the Design of Interventions

*Disorders of the first ray of the foot (defined as the hard and soft tissues of the first metatarsal, the sesamoids, and the phalanges of the great toe) are common, and therapeutic interventions to address these problems range from alterations in footwear to orthopedic surgery. Experimental verification of these procedures is often lacking, and thus, a computational modeling approach could provide a means to explore different interventional strategies. A three-dimensional finite element model of the first ray was developed for this purpose. A hexahedral mesh was constructed from magnetic resonance images of the right foot of a male subject. The soft tissue was assumed to be incompressible and hyperelastic, and the bones were modeled as rigid. Contact with friction between the foot and the floor or footwear was defined, and forces were applied to the base of the first metatarsal. Vertical force was extracted from experimental data, and a posterior force of 0.18 times the vertical force was assumed to represent loading at peak forefoot force in the late-stance phase of walking. The orientation of the model and joint configuration at that instant were obtained by minimizing the difference between model predicted and experimentally measured barefoot plantar pressures. The model were then oriented in a series of postures representative of push-off, and forces and joint moments were decreased to zero simultaneously. The pressure distribution underneath the first ray was obtained for each posture to illustrate changes under three case studies representing hallux limitus, surgical arthrodesis of the first ray, and a footwear intervention. Hallux limitus simulations showed that restriction of metatarsophalangeal joint dorsiflexion was directly related to increase and early occurrence of hallux pressures with severe immobility increasing the hallux pressures by as much as 223%. Modeling arthrodesis illustrated elevated hallux pressures when compared to barefoot and was dependent on fixation angles. One degree change in dorsiflexion and valgus fixation angles introduced approximate changes in peak hallux pressure by 95 and 22 kPa, respectively. Footwear simulations using flat insoles showed that using the given set of materials, reductions of at least 18% and 43% under metatarsal head and hallux, respectively, were possible.* [DOI: 10.1115/1.2768108]

*Keywords: finite element model, footwear, surgery, plantar pressure*

## Introduction

Complications of the first ray of the foot such as hallux limitus [1], hallux valgus [2], and arthritis [3] are frequently encountered in foot clinics. A majority of the conservative and surgical interventions for these conditions aim at reducing pain and stresses underneath the foot [4]. Therapeutic footwear is also routinely provided [5]. While in vivo and in vitro experimentations [6,7] have provided an in-depth understanding of the first ray biomechanics, certain aspects of therapeutic interventions, and surgical techniques, and rehabilitation can be addressed efficiently by computational modeling.

Finite element (FE) modeling can predict the plantar pressures underneath the foot and therefore allows simulations to be performed for a priori evaluation of therapeutic interventions [8]. The

[1]Corresponding author.
Contributed by the Bioengineering Division of ASME for publication in the JOURNAL OF BIOMECHANICAL ENGINEERING. Manuscript received October 17, 2005; final manuscript received February 27, 2007. Review conducted by Frank Yin.

  

analysis provides a cost effective computational framework to study anatomical structures of the foot during their interactions with the loading environment. A validated FE model can be used to investigate a variety of pathological conditions and the efficacy of corresponding interventions and therefore propose a limited yet pertinent design space for further experimentation.

Several two- and three-dimensional FE models of the foot have been developed to study various conditions of the foot. Two-dimensional simulations have been used to predict the stress state within the plantar soft tissue and the bones for different shoe conditions [9], to investigate the influence of tissue and insole thickness on the second metatarsal head (MTH) pressures [10], to simulate plantar pressure relief by using midsole plugs [8], and to evaluate the stress distribution under the MTH of diabetic and nondiabetic feet [11]. Three-dimensional models have been used to analyze ankle-foot orthoses [12], to determine the sensitivity of plantar pressure distribution to changes in soft-tissue properties [13], to quantify the stress distribution within the foot structure [14–16], to investigate the effect of total contact and flat insoles on plantar pressure redistribution [17], to investigate the mechanisms of ankle injury [18], and to provide insight into the functional consequences of bony alignment in the foot [19]. In many of these studies, there was limited or no representation of forefoot kinematics (e.g., movement of metatarsophalangeal joints). Additionally, most simulations addressed only a single stage of the stance phase of walking. Peak pressures under different regions of the foot (e.g., hallux versus MTH) vary at different stages of gait during which large changes in joint kinematics can occur.

The primary objective of this study was to develop kinematically realistic nonlinear large deformation FE models of the first ray to predict the plantar pressures underneath the first MTH and hallux during the late-stance phase of walking. The secondary objective was to illustrate the utilization of this model to simulate first ray pathologies and surgical and therapeutic interventions that aim at plantar pressure reduction underneath the first ray.

## Methods

**Finite Element Model.** The FE model of the first ray was developed from magnetic resonance (MR) images of 0.5 mm voxel size obtained from the right foot of a healthy male subject (94.5 kg, 1.88 m). Bone and soft-tissue contours were digitized using custom MATLAB (Mathworks, Inc., Natick, MA) code. Three-dimensional solid models of the soft tissue and the bones (first metatarsal, sesamoids, and distal and proximal phalanges) were obtained from these contours using PRO-E (PTC, Inc., Needham, MA), and further surface smoothing was carried out using RHINOCEROS (Robert McNeal & Associates) for appropriate meshing. Surface representations were then loaded into TRUEGRID (XYZ Scientific, Inc., Livermore, CA) for generation of high quality eight-node hexahedral meshes of the first ray structures. Models with various mesh densities (2,419, 10,416, 12,374, 15,239, and 34,884 elements) were created to perform a convergence analysis on plantar pressure predictions.

Bones were modeled as rigid, and soft tissue was modeled as a lumped incompressible hyperelastic material with strain energy density $U$ given by

$$U = \frac{2\mu}{\alpha^2}(\lambda_1^\alpha + \lambda_2^\alpha + \lambda_3^\alpha - 3) \tag{1}$$

where $\lambda_i (i=1-3)$ are the deviatoric principal stretches and $\mu$ and $\alpha$ are material coefficients that dictate the stress-strain response [20]. Values of $\mu$ (14.3 kPa) and $\alpha$ (7.3) were selected from prior studies [21] that used an inverse FE analysis of plantar tissues.

The kinematics of the first ray was defined by placing connectors at the metatarsophalangeal joint (MTPJ1) and the interphalangeal joint (IPJ1) (Fig. 1). Each connector had six degrees of freedom, where plantar/dorsiflexion of the joints was dominant and allowed to move within a normal range of motion (60 deg dorsiflexion, 60 deg plantarflexion) [22]. The remaining degrees of freedom were used solely for bone configuration changes to map experimental pressure data (as described below) and to model first ray abnormalities. The movement of the metatarsal bone with respect to the ground was also represented by additional six degrees of freedom that placed and oriented the whole FE model. The soft tissue was tied to bones, and sliding contacts were defined between deformable soft tissue and rigid floor and in cases of footwear simulations between deformable soft tissue and deformable insole and between deformable insole and rigid floor. These contact descriptions restrict contact surfaces to penetrate each other by allowing deformation and also sliding and separation in between. The coefficient of friction between contact surfaces was set to 0.5.

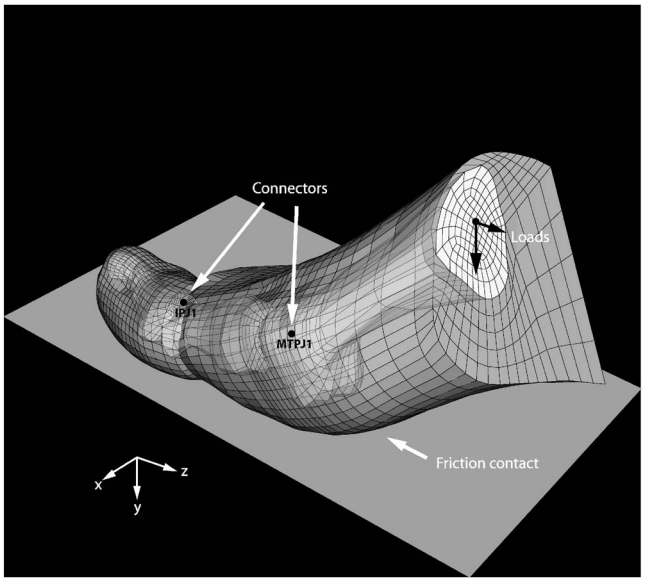


**Fig. 1 Initial position and loading of the foot for barefoot simulations. *x*, *y*, and *z* axes point medial, downward, and posterior, respectively. Connectors were placed at the center of rotation of each joint (MTPJ1, IPJ1). Contact with friction was defined between foot and the floor. Loads calculated from the experiments were applied at the base of MT.**

**Bone Alignment at the Initiation of Late Stance.** The foot was positioned on a rigid plate to approximately simulate the initiation of the late stance of walking when the ground reaction forces (GRFs) underneath the forefoot are largest. A vertical force of 294 N, calculated by integrating the experimental pressure data from a representative trial (see below for experimental details), and a horizontal force of 53 N, 18% of the vertical force, selected from the literature [23], were applied at the base of the metatarsal (Fig. 1). Adjustments to the orientation of the whole model as well as the relative alignment of bones were conducted by an optimization protocol that minimized the difference between the model predicted and experimentally measured pressures [24]. Given an initial configuration of the model, FE analysis calculated the contact pressures. Then, the model predicted pressure distribution and the experimental counterpart were aligned using centers of pressure as reference points. The model predicted pressures were interpolated at each sensor location, and the error function to be minimized was calculated as

$$\text{error} = \frac{1}{N}\sum_{i=1}^{N}(P_{\text{mod}_i} - P_{\text{exp}_i})^2 \tag{2}$$

where $N$ is the number of sensors, $P_{\text{exp}_i}$ is the measured pressure at sensor $i$, and $P_{\text{mod}_i}$ is the model predicted pressure as interpo-

**Table 1 Hyperfoam material coefficients used for a flat insole in the case study on therapeutic footwear. Material coefficients ($\mu$, $\alpha$, and $\nu$) were substituted into Eqs. (3) and (4) to obtain stress-strain response.**

| | Properties | | | | | |
|---|---|---|---|---|---|---|
| Materials | $\mu_1$ (MPa) | $\alpha_1$ | $\mu_2$ (MPa) | $\alpha_2$ | $\nu_1$ | $\nu_2$ |
| Firm Plastazote | 4.445 | 11.27 | −3.414 | 8.162 | −0.0628 | −0.2333 |
| Medium Plastazote | 0.7787 | 25 | −0.1669 | 6.023 | 0.0321 | −1.757 |
| Puff | 2.112 | 25 | −0.4144 | 4.017 | 0.0341 | −3.44 |
| Puff Lite | 0.8746 | 25 | −0.1272 | 0.7531 | 0.0512 | 1.389 |
| Poron | 0.333 | 14.63 | −0.00672 | 2.156 | 0.0432 | 0.5388 |

lated for sensor location $i$. Ten of the 18 degrees of freedom (sagittal and frontal plane rotations of the first metatarsal, three rotations and vertical translation of the proximal phalange defined by MTPJ1, and three rotations and vertical translation of the distal phalange represented by IPJ1) were calculated iteratively for the initiation of late-stance phase by this protocol. A MATLAB optimization algorithm using sequential quadratic programming [25] interacted with ABAQUS (Abaqus, Inc.) to solve the minimization problem. At each iteration, MATLAB code changed the ABAQUS input file to reflect the new bone configuration for the iteration, started the FE analysis, read the ABAQUS output file for model pressure distributions, and calculated the pressure prediction error (Eq. (2)). The algorithm terminated when the change in function value was less than 0.1 $kPa^2$ or the change in optimization variables was less than 0.01 mm or 0.01 deg. At the final configuration, the FE analysis also provided the required forces and moments to keep the degrees of freedom in this prescribed state. Plantarflexion moments of the MTPJ1 and IPJ1 were two of these required moments that were used for prospective simulations of the push-off phase. The protocol was conducted on the coarse mesh (2,419 elements) to reduce simulation time.

**Simulation of Push-Off.** Once the appropriate force and moments were determined, the push-off movement was simulated using a mesh with 10,416 elements and by defining a series of steps that solve the static model in a new kinematic configuration at progressive frames in time, similar to the collection of experimental data, but at a much lower frequency. Further increase in mesh density only resulted in an 8% change in peak MTH pressures and a 2% change in peak hallux pressure at the initiation of push-off. At the initiation of late-stance phase, plantarflexion moments of 5.59 and 0.47 N m, as calculated from the optimization protocol, were applied to MTJ1 and IPJ1, respectively. Push-off was simulated by monotonically decreasing the forces applied to the metatarsal base and the joint moments to zero at toe off. A 45 deg rotation of the metatarsal was also imposed simultaneously to simulate the gross movement of the foot during push-off [26]. All other degrees of freedom were kept at their optimized values.

**Experiments.** Barefoot plantar pressures were collected at 100 Hz with a resolution of 0.25 $cm^2$ using an Emed-X capacitive sensor array (Novel Gmbh, Munich, Germany). Five trials were obtained with the subject walking at a self-selected pace. The pressure data were read into MATLAB, and the total vertical GRF was plotted for the whole duration of stance phase. The frame of interest was chosen under the assumption that late stance began when the forefoot GRF reached a peak. The first ray region of interest was isolated from the late-stance pressure frame, and pressures were integrated to calculate total first ray vertical force. The vertical force value for a representative trial (294 N) was used to load the FE model. The plantar pressure data for this time frame of the representative trial were used for optimization. Plantar pressure data measured from the entire late-stance phase were used for validation.

**Case Study 1: Hallux Limitus.** A common pathological condition of the first ray is hallux limitus [1] in which MTPJ1 motion is limited, which, in the extreme case, reduces to an immobile hallux. The condition leads to high plantar pressures, which can be relieved through a variety of interventions [27,28] that can be simulated by our model. As a case study, the first ray model was adjusted to represent hallux limitus by restraining the appropriate degrees of freedom. The simulation protocol included an increase in passive stiffness defined with connector properties and a "locking angle" of MTPJ1. The locking angle restricted MTPJ1 from any further extension. The stiffness properties were obtained from the literature [22], and the values of locking angle were varied from a normal joint (60 deg dorsiflexion) to severe hallux limitus (0 deg dorsiflexion). Peak MTH and hallux pressures and the timing of peak hallux pressure during the push-off phase of walking were obtained from the model output.

**Case Study 2: Arthrodesis of the First Ray.** The success rate of first ray arthrodesis (fusion) for severe hallux valgus and varus is well documented in the literature [29–31]. While excellent clinical results have been reported following MTPJ1 arthrodesis, less is known regarding the effects of fusion on plantar pressure distribution and the optimal configuration of the fusion procedure [32,33]. The first ray model was used to model the postsurgical state that allowed the position of the MTPJ1 to be fixed in different angles of dorsiflexion (30 deg, 36 deg, and 40 deg) while keeping the valgus angle at 15 deg. Different valgus fixation angles (10 deg, 15 deg, 20 deg, 25 deg, and 30 deg) were also investigated at a constant dorsiflexion fixation angle (36 deg). The postsurgical kinematics of the metatarsal was also modified to reflect the reduced ankle plantar flexion at toe off reported in the literature [32]. The push-off phase of gait was simulated for each fixation set, and peak MTH and hallux pressures were obtained.

**Case Study 3: Therapeutic Footwear.** The FE model of the first ray was modeled in contact along with a 15 mm thick deformable flat insole to investigate the influence of five different insole materials on plantar pressure redistribution. The insole was meshed with eight-node hexahedral elements using TRUEGRID. Insoles were assigned hyperfoam material properties with the strain energy function given by

$$U = \sum_{i=1}^{2} \frac{2\mu_i}{\alpha_i^2}\left[\lambda_1^{\alpha_i} + \lambda_2^{\alpha_i} + \lambda_3^{\alpha_i} - 3 + \frac{1}{\beta_i}(J_{el}^{-\alpha_i\beta_i} - 1)\right] \tag{3}$$

where

$$\beta_i = \frac{\nu_i}{1 - 2\nu_i} \tag{4}$$

$\lambda_{1-3}$ are the principal stretches, and $\mu$, $\alpha$, and $\nu$ (the effective Poisson's ratio) are the material properties [20]. Material specific parameters are given in Table 1 and were determined from the fits to uniaxial compression data. Frictional contacts with a coefficient

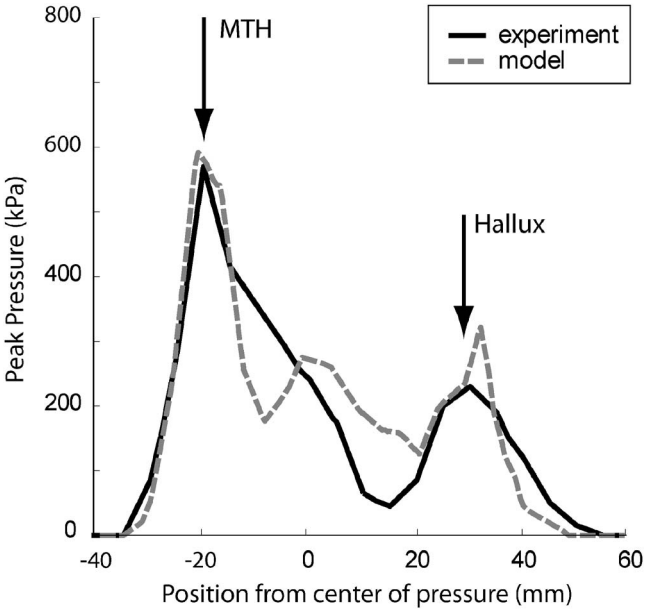


**Fig. 2 Peak pressures along the longitudinal axis of the first ray at initiation of late stance. Experimental measurements from a representative trial are shown in addition to model predicted plantar pressures using the coarse mesh following optimal bone alignment. Arrows represent the location of the MTH and hallux.**

of 0.5 were modeled between the foot and insole and the insole and the floor. The posterior edge of the insole was tied to the metatarsal base to simulate the movement of the insole with the foot, while the anterior end was kept free. Plantar pressures were obtained from push-off simulations, and relative changes in peak MTH and hallux pressures were calculated and compared to model predictions of barefoot walking.

## Results

Bone alignments were calculated using the optimization procedure described above on a representative trial of plantar pressure distributions from five experimental trials. For the representative trial, plantarflexion angles of the MTPJ1 and IPJ1 at the time of peak force were calculated as 2.1 deg and 6.3 deg, and the moments required to hold these positions were 5.59 N m for the MTPJ1 and 0.47 N m for IPJ1. For the same trial, the root mean square error of coarse model predicted pressures was 59 kPa (10% maximum pressure) at the initiation of stance phase (Fig. 2).

Peak pressures at the hallux and MTH during the late-stance phase as predicted by the fine mesh model (10,416 elements) were higher than those measured experimentally (Fig. 3(*a*)). It should be recalled that the coarse model (2,419 elements) was used for optimization and barefoot simulations only. Hallux peak pressure occurred later in the push-off phase than peak MTH1 pressure. In general, the timings of model predictions were in good agreement with experiment values (Fig. 3(*b*)).

Simulations of hallux limitus showed that hallux peak pressure was dependent on dorsiflexion locking angle and increased significantly as the joint range of motion was restricted (Fig. 4(*a*)). Regardless of increased stiffness properties, the dorsiflexion of the MTPJ1 during the push-off phase reached the imposed limits for locking angles less than 25 deg. Peak hallux pressures occurred earlier in the models with limited MTPJ1 mobility (Figure 4(*b*)). Approximately 25 deg dorsiflexion of MTPJ1 appeared to be sufficient to keep peak pressures close to normal under the kinematic conditions modeled. Figure 4(*a*) illustrates a constant peak pressure of 850 kPa under the MTH for all locking angles.

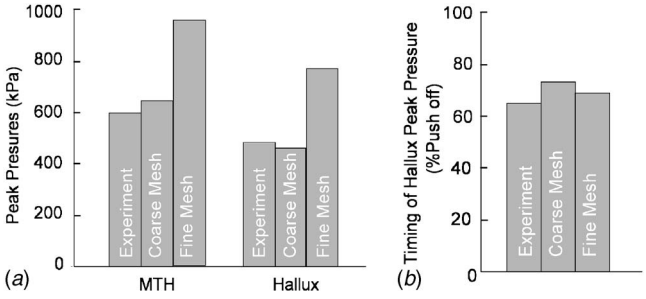


**Fig. 3 Validation of the model. (*a*) Barefoot plantar pressures under MTH and hallux obtained experimentally and from the model (coarse and fine). (*b*) Timing of hallux peak pressure from experiments and model (coarse and fine) during push-off phase of walking.**

Conventional fixation angles for MTPJ1 arthrodesis (dorsiflexion=36 deg, valgus=15 deg) demonstrated markedly elevated hallux pressures compared to normal barefoot values. Table 2 shows peak hallux pressure values for various postsurgical MTPJ1 fixation angles expressed as a percentage of conventional fixation angles (hallux pressure at 15 deg values and 36 deg dorsiflexion is 1038 kPa). As expected, increments in the dorsiflexion fixation angle decreased peak hallux pressure; 1 deg increase in dorsiflexion resulted in an average of 9% drop in peak pressure. Increasing the valgus angle at fixation increased peak hallux pressure; within the simulated range of fixation angles, 1 deg increase in valgus angle elevated the peak pressure by approximately 2%.

The introduction of a flat insole underneath the first ray led to a reduction of peak pressures compared to the barefoot walking simulation for all insole materials (Fig. 5(*a*)). Poron® resulted in the largest pressure reduction, 68% at the hallux and 69% underneath the MTH (Fig. 5(*b*)). At least 18% and 43% pressure reductions were obtained for the MTH and the hallux, respectively, regardless of the insole material selected.

## Discussion

A three-dimensional FE model of the first ray has been developed to predict contact pressures underneath the first MTH and the hallux. The model incorporates kinematics of the metatarsophalangeal and interphalangeal joints, nonlinear material properties of the soft tissue, and contact definitions between the foot, footwear, and floor. The modeling framework allows for realistic simulations of the push-off phase of walking during which the forefoot is loaded maximally. The computational approach outlined in this study provides a tool for the design of first ray interventions as demonstrated by the case studies of hallux limitus, first ray arthrodesis, and therapeutic footwear.

**Base Line Barefoot Simulations.** The uncertainty of joint loading was solved by utilizing an optimization algorithm, which mapped the model predicted barefoot pressures to those measured experimentally (Fig. 2). This novel approach calculated joint configuration (joint angles) at the initiation of push-off, which also corresponded to a loading state (joint moments) of the metatarsophalangeal and interphalangeal joints. This loading state—rather than a prescribed joint angle—was then applied to allow relative movement between the bones during push-off.

As the average interface areas of the elements in the coarse model were approximately similar to the area of the pressure sensor used in the experiments (22 $mm^2$ for model and 25 $mm^2$ for experiment), model predictions for the coarse mesh were in good agreement to the experimental plantar pressure data. On the other hand, due to smaller interface areas of the fine mesh (12 $mm^2$), the fine mesh overpredicted the experimental plantar pressures. Nevertheless, relative load distributions between the hallux and MTH were similar in all cases: the ratios of hallux to MTH peak

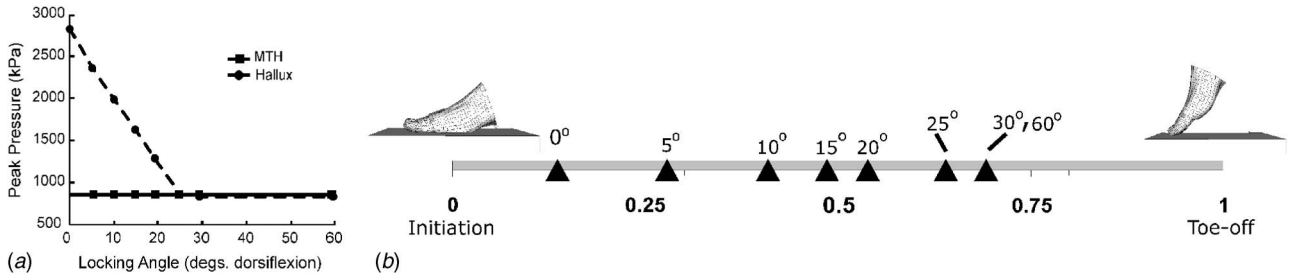


**Fig. 4 Simulation results for hallux rigidus. (*a*) Peak pressure under MTH1 and hallux versus locking angle of MTPJ. (*b*) The timing of peak hallux pressure predicted for various locking angles (indicated by labeled arrows). The horizontal line shows percentage of the late-stance phase, starting at peak forefoot force.**

pressures were 79% in experiments, 81% with the coarse mesh, and 81% with the fine mesh. Most notably, timing of peak hallux pressure was predicted very well, illustrating the appropriate kinematic modeling of the metatarsophalangeal joint. This finding illustrates the importance of considering not only spatial but also temporal distribution of plantar pressures while designing an intervention for foot complications. Previous foot modeling studies have provided [13,17] or had the potential to provide [19] spatial distribution of plantar pressures underneath the first ray but lacked the capacity for prediction of temporal changes. Previous investigations, which have attempted to predict both spatial and temporal pressure distributions underneath the foot, did not include the kinematics of the metatarsophalangeal joint. This is clearly influential in the load distribution between the hallux and the first MTH [14,15].

**Model Limitations.** The results of this study should be interpreted with regard to the limitations inherent to the modeling approach taken. These limitations can be grouped into three categories: (i) representation of first ray only, (ii) subject-specific model development, and (iii) assumptions used to build and solve the model.

The present model was solely based on the first ray in order to focus on the complications of the metatarsophalangeal joint and the hallux. Therefore, the model is not suitable for the investigation of interventions that will redistribute the plantar loading among the MTHs. The three-dimensional nature of the model, however, allows out of plane simulations such as hallux valgus that would not be possible by a simple plane strain model. Also, the prediction of load redistribution between the first MTH and hallux following an intervention is within the capabilities of the model.

The model is a subject-specific representation of a healthy person without foot deformities. Nevertheless, the results obtained using this model provide a good understanding of the underlying principles of first ray complications and interventions. Complicated feet with excessive deformities will likely require models developed specifically for the patient, and the modeling principles established in this study can be used as a guideline.

A variety of assumptions may contribute to prediction errors in peak pressure magnitudes. First, the sesamoids were incorporated into the MTH to simplify the kinematic description of bones. The sesamoids have been reported to move along with the proximal phalanx [34]. While it is possible to model these bones individually and incorporate their kinematics, generating FE meshes of these small sized bones is not practical. Second, the soft tissue was assumed to be lumped (that is, no distinction was made between fat, tendon, muscle, etc.), and the properties of the heel pad [21], probably a softer material representation for the forefoot, were used to describe its nonlinearly elastic behavior. The third source of error relates to manual segmentation and smoothing of the surfaces, which may have influenced the bone and soft-tissue curvatures and therefore changed peak pressure predictions. Change in mesh density also caused differences in peak pressures, yet the prediction errors were unidirectional; an increased mesh density caused higher peak pressures (Fig. 3). A horizontal force was implemented in the first ray model, since it is an important component of the gait cycle as it acts as the propelling force during push-off phase of walking. Although this force was not recorded during plantar pressure measurements, it was assumed based on the ratio of anterior-posterior to vertical GRFs extracted from the normative data given by Chao et al. [23] at peak forefoot force instant of gait.

All of the above limitations can influence the magnitudes of predicted peak MTH and hallux pressures, but the relative difference between these regions and comparisons following an intervention are less likely affected due to the systematic nature of these assumptions. Therefore, the model results should not be accepted in an absolute sense; rather, the percentage change caused by an alteration in condition should be considered. For this reason, in each case study, we have attempted to outline the changes in peak pressures with reference to the barefoot simulation with the same sesamoid modeling, tissue properties, vertical and horizontal loadings, mesh density, and surface descriptions.

**Hallux Limitus Simulations.** Hallux limitus has been shown experimentally to result in abnormally high plantar pressure under the hallux [35]. Our simulation approach was capable of reproducing this clinical observation and also illustrated the dependency of hallux peak pressure on the degree of immobility (Fig. 4). Notable in our simulations is that the MTH pressure was not influenced by the stiffness characteristics of the metatarsophalangeal joint. This prediction is due to timing of the peak MTH pressure (initiation of push-off), which occurs at an instant that the metatarsophalangeal joint is approximately at its neutral position, which is well below the limits induced by hallux limitus [22]. At

**Table 2 Change in peak hallux pressures for postsurgical MTPJ1 fixation with respect to that of conventional fixation angles. Peak hallux pressures at pre- and postsurgery (conventional fixation angles) were 773 and 1038 kPa, respectively.**

| Angle (deg) | | Valgus | | | | |
|---|---|---|---|---|---|---|
| Dorsiflexion | | 10 | 15 | 20 | 25 | 30 |
| | 30 | — | 62% | — | — | — |
| | 36 | –9% | **0**% | 13% | 26% | 34% |
| | 40 | — | 28% | — | — | — |

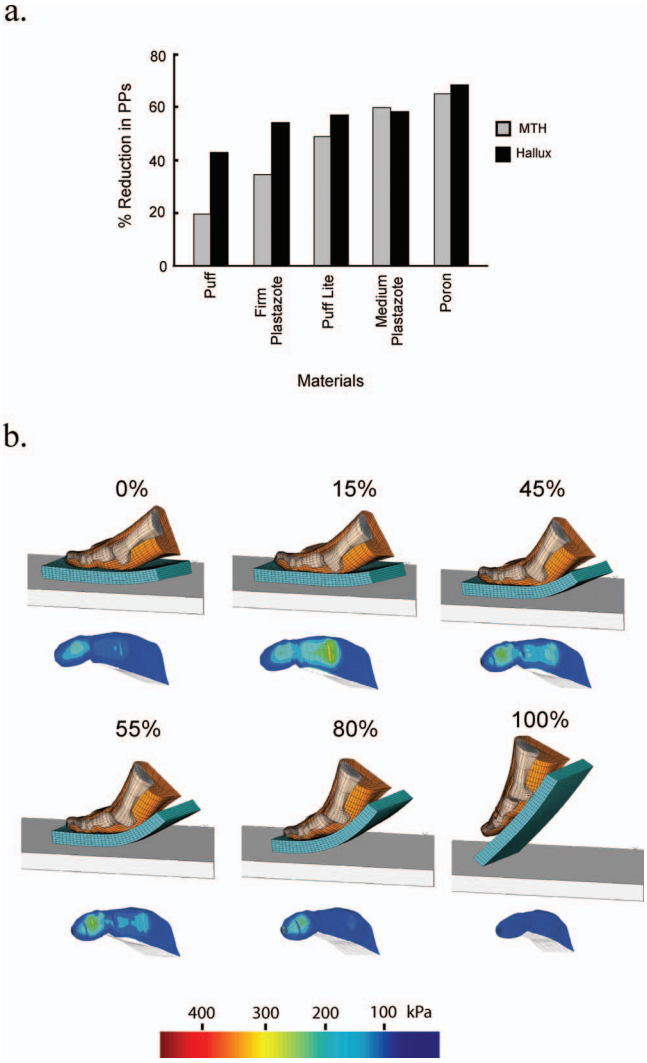


**Fig. 5 Simulation results for footwear interventions. (*a*) Reduction in plantar pressure under MTH and hallux for five different insole materials. (*b*) Late-stance simulation using flat insole made out of Poron.**

that angle, the passive joint moment dictated by MTPJ1 stiffness properties is relatively small compared to the moment applied to the joint. Elevated peak hallux pressures predicted by our simulations confirm experimental findings and provide a framework upon which interventions to relieve hallux pressures can further be tested. For example, footwear designs such as rocker bottom shoes can be explored to compensate for the altered kinematics and to redistribute the load to the remainder of the first ray.

**Simulations of Arthrodesis of the First Ray.** Although established as a pain relieving surgery, arthrodesis of the first metatarsophalangeal joint elevates hallux pressures considerably [32]. Simulation results revealed a similar trend but, most importantly, quantified the sensitivity of peak hallux pressures to surgical parameters (dorsiflexion and valgus fixation angles). A critical finding of this study is that conventional fixation angles (36 deg dorsiflexion and 15 deg valgus) are not necessarily optimal for reduced plantar pressures. A higher dorsiflexion angle and/or a lower valgus angle may be more beneficial in this respect. On the other hand, increasing dorsiflexion fixation angle or decreasing valgus fixation angle might have consequences for cosmesis, dynamic function, and load carrying capacity of the first ray. In addition to surgery, other interventions can be prescribed to compensate for changes in mobility, and these can be tested a priori by the FE model of the first ray.

**Therapeutic Footwear Simulations.** Therapeutic footwear has been found to be an effective conservative treatment to relieve plantar pressures underneath the foot in certain conditions [36,37]. Our simulations show how different flat insole materials can reduce first ray peak pressures. When compared to barefoot, reductions up to 69% were found (Fig. 5), similar to those reported by the experimental study of Bus et al. [38] for a 9.5 mm thick flat PPT® insole (approximately 67% reduction under the first MTH and 59% reduction under the hallux). Kinematic modeling of the insole by tying the posterior end to the base of the metatarsal allowed realistic simulations and ensured that the insole remained in contact with the foot. Model changes were simply handled by updating the material properties for the insole and running simulations again. This highlights the indispensable advantage of the computational approach over experimental testing that requires time and effort to manufacture and test individual insole designs. Poron, the softest material, was found to be the most effective to reduce peak pressures when used for a flat insole. Studies that measured plantar pressures while stepping on flat insole materials showed a similar trend between pressure relief and material softness [39–41]. It is possible to expand upon these simulations by testing multilayered insoles and varying insole thickness and contours, as in a custom molded insole.

In summary, an effective computational platform to simulate pathological conditions of the first ray and to explore therapeutic and surgical procedures to resolve these conditions has been developed. We have shown that it is possible to focus on first ray interventions without the increased complexity and solution time of a whole foot model. In addition, the modeling approach utilized in this study is equally applicable to forefoot models currently under development in our laboratory. We expect that such models will realistically simulate the redistribution of plantar pressure between MTHs and will be able to address interventions that aim to alter this three-dimensional pressure distribution.

## Acknowledgment

This study was funded by the NIH Grant No. 5R01 HD037433. One of the authors (S.P.B.) was supported by the matching dissertation grant of the International Society of Biomechanics and another author (M.P.) was supported by NIH Grant No. T32 EB04314.

## References

[1] Dananberg, H. J., 1986, "Functional Hallux Limitus and Its Relationship to Gait Efficiency," J. Am. Podiatr. Med. Assoc., **76**(11), pp. 648–652.
[2] Coughlin, M. J., 1984, "Hallux Valgus: Causes, Evaluation, and Treatment," Postgrad Med., **75**(5), pp. 174–178.
[3] Shereff, M. J., and Baumhauer, J. F., 1998, "Hallux Rigidus and Osteoarthrosis of the First Metatarsophalangeal Joint," J. Bone Jt. Surg., Am. Vol., **80**(6), pp. 898–908.
[4] Yu, G. V., and Gorby, P. O., 2004, "First Metatarsophalangeal Joint Arthrodesis," Clin. Podiatr Med. Surg., **21**, pp. 65–96.
[5] Raspovic, R., Newcombe, L., Lloyd, J., and Dalton, E., 2000, "Effect of Customized Insoles on Vertical Plantar Pressures in Sites of Previous Neuropathic Ulceration in the Diabetic Foot," Diabetic Foot, **10**, pp. 133–138.
[6] Jacob, H. A., 2001, "Forces Acting in the Forefoot During Normal Gait—An Estimate," Clin. Biomech. (Bristol, Avon), **16**(9), pp. 783–792.
[7] Shereff, M. J., Bejjani, F. J., and Kummer, F. J., 1986, "Kinematics of the First Metatarsophalangeal Joint," J. Bone Jt. Surg., Am. Vol., **68**(3), pp. 392–398.
[8] Erdemir, A., Saucerman, J. J., Lemmon, D., Loppnow, B., Turso, B., Ulbrecht, J. S., and Cavanagh, P., "Local Plantar Pressure Relief in Therapeutic Footwear: Design Guidelines From Finite Element Models," J. Biomech., 2005, Vol. **38**(9), pp. 1798–1806.
[9] Nakamura, S., Crowninshield, R. D., and Cooper, R. R., 1981, "An Analysis of Soft Tissue Loading in the Foot—A Preliminary Report," Bull. Prosthet. Res., **10–35**, pp. 27–34.
[10] Lemmon, D., Shiang, T. Y., Hashmi, A., Ulbrecht, J. S., and Cavanagh, P. R., 1997, "The Effect of Insoles in Therapeutic Footwear—A Finite Element Approach," J. Biomech., **30**(6), pp. 615–620.
[11] Gefen, A., 2003, "Plantar Soft Tissue Loading Under the Medial Metatarsals in

the Standing Diabetic Foot," Med. Eng. Phys., **25**(6), pp. 491–499.
[12] Chu, T. M., Reddy, N. P., and Padovan, J., 1992, "Three Dimensional Finite Element Stress Analysis of the Polypropylene Ankle-Foot Orthosis," Adv. Bioeng., **22**, pp. 407–409.
[13] Cheung, J. T., Zhang, M., Leung, A. K., and Fan, Y. B., "Three-Dimensional Finite Element Analysis of the Foot During Standing—A Material Sensitivity Study," J. Biomech., 2005, **38**, pp. 1045–1054.
[14] Chen, W. P., Tang, F. T., and Ju, C. W., 2001, "Stress Distribution of the Foot During Mid-Stance to Push-Off in Barefoot Gait: A 3-D Finite Element Analysis," Clin. Biomech. (Bristol, Avon), **16**(7), pp. 614–620.
[15] Gefen, A., Megido-Ravid, M., Itzchak, Y., and Arcan, M., 2000, "Biomechanical Analysis of the Three-Dimensional Foot Structure During Gait: A Basic Tool for Clinical Applications," J. Biomech. Eng., **122**, pp. 630–639.
[16] Thomas, V. J., Patil, K. M., and Radhakrishnan, S., 2004, "Three-Dimensional Stress Analysis for the Mechanics of Plantar Ulcers in Diabetic Neuropathy," Med. Biol. Eng. Comput., **42**(2), pp. 230–235.
[17] Chen, W. P., Ju, C. W., and Tang, F. T., 2003, "Effects of Total Contact Insoles on the Plantar Stress Redistribution: A Finite Element Analysis," Clin. Biomech. (Bristol, Avon), **18**(6), pp. S17–S24.
[18] Bandak, F. A., Tannous, R. E., and Toridis, T., 2001, "On the Development of an Osseo-Ligamentous Finite Element Model of the Human Ankle Joint," Int. J. Solids Struct., **38**, pp. 1681–1697.
[19] Camacho, D. L., Ledoux, W. R., Rohr, E. S., Sangeorzan, B. J., and Ching, R. P., 2002, "A Three-Dimensional, Anatomically Detailed Foot Model: A Foundation for a Finite Element Simulation and Means of Quantifying Foot-Bone Position," J. Rehabil. Res. Dev., **39**(3), pp. 401–410.
[20] *Abaqus Theory Manual*, Abaqus, Providence, RI, 2003.
[21] Erdemir, A., Viveiros, M. L., and Cavanagh, P. R., 2003, "A Numerical-Experimental Approach for Characterizing Subject Specific Hyperelastic Properties of the Heel Pad," *ASME Summer Bioengineering Conference*, Key Biscayne, FL, June 25–29.
[22] Birke, J. A., Cornwall, M. A., and Jackson, M., 1988, "Relationship Between Hallux Limitus and Ulceration of the Great Toe," J. Orthop. Sports Phys. Ther., **10**(5), pp. 172–176.
[23] Chao, E. Y., Laughman, R. K., and Schneider, E., 1983, "Normative Data of Knee Joint Motion and Ground Reaction Forces in Adult Level Walking," J. Biomech., **16**(3), pp. 219–233.
[24] Erdemir, A., Petre, M., Budhabhatti, S., and Cavanagh, P. R., 2004, "Optimization of Bone Alignment to Reproduce Plantar Pressures in a Subject-Specific Finite Element Foot Model," *28th Annual Meeting of the American Society of Biomechanics*, Portland, OR, Sept. 8–11.
[25] Schittkowski, K., 1985, "NLQPL: A FORTRAN-Subroutine Solving Constrained Nonlinear Programming Problems," Ann. Operat. Res., **5**, pp. 485–500.
[26] Fauth, A. R., Hamel, A. J., and Sharkey, N. A., 2004, "In Vitro Measurements of First and Second Tarsometatarsal Joint Stiffness," Journal of Applied Biomechanics, **20**, pp. 14–24.
[27] Dannels, E., 1989, "Neuropathic Foot Ulcer Prevention in Diabetic American Indians With Hallux Limitus," J. Am. Podiatr. Med. Assoc., **79**(9), pp. 447–450.
[28] van Schie, C. H., Whalley, A., Vileikyte, L., Wignall, T., Hollis, S., and Boulton, A. J., 2000, "Efficacy of Injected Liquid Silicone in the Diabetic Foot to Reduce Risk Factors for Ulceration: A Randomized Double-Blind Placebo-Controlled Trial," Diabetes Care, **23**(5), pp. 634–638.
[29] Coughlin, M. J., 1990, "Arthrodesis of the First Metatarsophalangeal Joint," Orthop. Rev., **19**(2), pp. 177–186.
[30] Coughlin, M. J., 1990, "Arthrodesis of the First Metatarsophalangeal Joint With MiniFragment Plate Fixation," Orthopedics, **13**(9), pp. 1037–1044.
[31] Southgate, J. J., and Urry, S. R., 1997, "Hallux Rigidus: The Long-Term Results of Dorsal Wedge Osteotomy and Arthrodesis in Adults," J. Foot Ankle Surg., **36**(2), pp. 136–140.
[32] DeFrino, P. F., Brodsky, J. W., Pollo, F. E., Crenshaw, S. J., and Beischer, A. D., 2002, "First Metatarsophalangeal Arthrodesis: A Clinical, Pedobarographic and Gait Analysis Study," Foot Ankle Int., **23**(6), pp. 496–502.
[33] Buck, P., Morrey, B. F., and Chao, E. Y. S., 1987, "The Optimum Position of Arthrodesis of the Ankle," J. Bone Jt. Surg., Am. Vol., **69-A**(7), pp. 1052–1062.
[34] Kuwano, T., Nagamine, R., Sakaki, K., Urabe, K., and Iwamoto, Y., 2002, "New Radiographic Analysis of Sesamoid Rotation in Hallux Valgus: Comparison With Conventional Evaluation Methods," Foot Ankle Int., **23**(9), pp. 811–817.
[35] Shrader, J. A., and Siegel, K. L., 2003, "Nonoperative Management of Functional Hallux Limitus in a Patient With Rheumatoid Arthritis," Phys. Ther., **83**(9), pp. 831–843.
[36] Maciejewski, M. L., Reiber, G. E., Smith, D. G., Wallace, C., Hayes, S., and Boyko, E. J., 2004, "Effectiveness of Diabetic Therapeutic Footwear in Preventing Reulceration," Diabetes Care, **27**(7), pp. 1774–1782.
[37] Cavanagh, P. R., 2004, "Therapeutic Footwear for People With Diabetes," Diabetes/Metab. Rev., **20**(1), pp. S51–S55.
[38] Bus, S. A., Ulbrecht, J. S., and Cavanagh, P. R., 2004, "Pressure Relief and Load Redistribution by Custom-Made Insoles in Diabetic Patients With Neuropathy and Foot Deformity," Clin. Biomech. (Bristol, Avon), **19**(6), pp. 629–638.
[39] Sanfilippo, P. B., II, Stess, R. M., and Moss, K. M., 1992, "Dynamic Plantar Pressure Analysis: Comparing Common Insole Materials," J. Am. Podiatr. Med. Assoc., **82**(10), pp. 507–513.
[40] McPoil, T. G., and Cornwall, M. W., 1992, "Effect of Insole Material on Force and Plantar Pressures During Walking," J. Am. Podiatr. Med. Assoc., **82**(8), pp. 412–416.
[41] Leber, C., and Evanski, P. M., 1986, "A Comparison of Shoe Insole Materials in Plantar Pressure Relief," Prosthet. Orthot Int., **10**(3), pp. 135–138.